Ni- and PtNi-catalysts supported on Al2O3 for acetone steam reforming: Effect of the modification of support with Ce, La and Mg

ARTICLE *in* CATALYSIS TODAY · SEPTEMBER 2014

Impact Factor: 3.89 · DOI: 10.1016/j.cattod.2014.07.036

5 AUTHORS, INCLUDING:

R. Guil-Lopez
Spanish National Research Council
36 PUBLICATIONS **920** CITATIONS
SEE PROFILE

Adel Ismail
Central Metallurgical Research and Develo…
41 PUBLICATIONS **888** CITATIONS
SEE PROFILE

Catalysis Today 242 (2015) 60–70

Contents lists available at ScienceDirect

Catalysis Today

journal homepage: www.elsevier.com/locate/cattod

Ni- and PtNi-catalysts supported on Al_2O_3 for acetone steam reforming: Effect of the modification of support with Ce, La and Mg

R.M. Navarro[a,*], R. Guil-Lopez[a,**], A.A. Ismail[b,c], S.A. Al-Sayari[b], J.L.G. Fierro[a]

[a] Grupo de Energía y Química Sostenibles, ICP-CSIC, C/Marie Curie 2, Cantoblanco, 28049 Madrid, Spain
[b] Advanced Materials and Nanoresearch Centre, Najran University, Najran 11001, Saudi Arabia
[c] Advanced Materials Department, Central Metallurgical R&D Institute, CMRDI, Helwan 11421, Egypt

ARTICLE INFO

Article history:
Received 10 March 2014
Received in revised form 4 July 2014
Accepted 18 July 2014
Available online 5 September 2014

Keywords:
Ni- and Pt-catalysts
La-, Mg- or Ce-alumina modified
Hydrogen production
Bio-oil
Acetone reforming

ABSTRACT

Hydrogen production from acetone steam reforming was studied using bimetallic PtNi catalysts supported on modified alumina. La-, Ce- and Mg-oxides were used as support modifiers in order to neutralize acidity and/or to improve water adsorption and OH^- surface mobility of Al_2O_3 support. Characterization of the sample showed that metal-support interactions and the size of metallic Ni at surface differ depending on the oxide added to the alumina support. Reforming activity on Ni and Pt–Ni supported on X-modified-Al_2O_3 catalysts (X = La, Ce, or Mg) showed that both metal and support, play an essential role in the catalytic behavior on the steam reforming of acetone. The sequence of gasification capacity over monometallic samples (Ni/LaAl > Ni/MgAl > Ni/CeAl) points out that acidity of supports participates in the acetone reforming mechanism over these catalysts. Addition of Pt to monometallic Ni catalysts only has a beneficial effect on the reforming capacity of the Ni/LaAl sample. Improvement in the reforming capacity of the PtNi/LaAl catalyst is believed to be a consequence of the promoting effect of Pt that leads to an increase in the stability of metallic Ni particles on catalyst surface together with the ability of Pt to enhance the mobility of the H-atoms formed in the reaction could help the gasification of carbon precursors formed during the reforming of acetone.

1. Introduction

The production of hydrogen from biomass is receiving increased attention as a potential source of renewable energy respect to global issues of sustainable energy. Hydrogen could be produced from biomass by two main thermochemical methods: (i) biomass gasification, and (ii) catalytic steam reforming of pyrolysis oils (bio-oils) [1]. Bio-oils are easier to handling and transport than biomass and therefore make the process of hydrogen production from these bio-oils an interesting alternative to gasification processes [2–5]. Depending on the biomass feedstock and the pyrolysis conditions employed, the composition of bio-oil varied but it mainly consists in a mixture of aliphatic and aromatic oxygenated compounds, such as acids, ketones, alcohols, phenols and sugars [6,7]. In order to get a better understanding of the chemical process occurring during the steam reforming of the whole bio-oil, a number of studies have been appeared in the literature focused on the steam reforming of bio-oil model compounds. Most of the studies have been focused on the reforming of acetic acid [8–11], whereas acetone steam reforming (Eq (1)) has been less studied in spite that this compound could be the model of the carbonyl-containing compounds present in bio-oils (ketones).

$$CH_3COCH_3 + 5H_2O \rightarrow 3CO_2 + 8H_2 \quad (1)$$

Moreover, acetone reforming process in the key for the reforming of acetic acid, due to acetone is the most important intermediate during the acetic acid reforming process [9–11]. Thus, the optimization of the acetone reforming process would favor the acetic acid reforming.

In the literature, the steam reforming of oxygenated compounds has been performed over catalyst systems using Ni [12–14] and Pt [15,16] as active phases deposited on different oxide supports (Al_2O_3, Al_2O_3-CaO, ZrO_2 and CeO_2) to improve both thermal stability and resistance to coke formation. The Ni-ability to C—C bond breaking and its low cost make the Ni as the best active phase for

* Corresponding author at: Instituto de Catálisis y Petroleoquímica, CSIC, C/ Marie Curie 2, Cantoblanco, 28049 Madrid, Spain. Tel.: +34 915854774; fax: +34 915854760.
** Corresponding author at: Instituto de Catálisis y Petroleoquímica, CSIC, C/ Marie Curie 2, Cantoblanco, 28049 Madrid, Spain. Tel.: +34 915854759; fax: +34 915854760.
E-mail addresses: r.navarro@icp.csic.es (R.M. Navarro), rut.guil@icp.csic.es (R. Guil-Lopez).

http://dx.doi.org/10.1016/j.cattod.2014.07.036
0920-5861/

the acetone steam reforming catalysts, although the coke formation facility for the Ni-based catalysts represents an important problem in bio-oil reforming on Ni based catalysts. In a previous work [17], we have reported that the addition of small amounts of Pt to Ni/La-Al_2O_3 catalyst enhances the gasification capacity respect to the monometallic Ni counterpart, achieving the bimetallic PtNi catalyst almost complete gasification of the acetone. The characterization results over bimetallic PtNi catalyst revealed that the presence of platinum increases the reducibility and surface exposure of metallic Ni. Additionally, the better ability of Pt to enhance the mobility of the H-atoms formed in the reaction could help the gasification of carbon precursors. The combination of both effects is interpreted as responsible for the higher reforming capacity of the bimetallic PtNi catalyst.

On the other hand, the nature of support strongly influences the catalytic performance of supported Ni catalyst for the steam reforming of oxygenated compounds since the interactions between Ni- or PtNi-active phases with the support affect the catalytic properties of the active phase. Moreover, the supports can play an important role or even participate in the reaction. Alumina is often used as support for Ni based reforming catalysts due to its robustness and chemical stability under the most of the reaction conditions. Nevertheless, the acidity of Al_2O_3 support favors the coke formation by polymerization or oligomerization reactions and catalyses the aldol condensation, which causes catalyst deactivation by deposition of intermediates reactions [18,19]. Thus, basic promoters supported on alumina surface are required to improve the catalysts performances in these kinds of reactions to favor water adsorption and OH surface mobility. Addition of alkaline earth oxides (MgO, CaO) is widely used in reforming formulations to neutralize acidity of Al_2O_3. Another approach consists in the addition of lanthanide oxides since these oxides are known promoters of carbon removal from metallic surfaces [20–22].

With this background, the aim of the present work was to study the effect of addition of La, Mg or Ce oxides on the behavior of alumina-supported Ni- and PtNi-catalysts in the production of hydrogen by steam reforming of acetone. Careful investigations of the structure of the catalysts were performed in fresh and used state to understand the relationship between activity and their structural and surface characteristics.

2. Experimental

2.1. Catalysts preparation

Ni and Pt–Ni supported on X-modified-Al_2O_3 catalysts (X = La, Ce, or Mg) were prepared by subsequent wet impregnation method. X-Al_2O_3 supports were prepared by wet impregnation of a commercial γ-Al_2O_3 (*Alfa Aesar*, S_{BET} = 212 m^2/g) with aqueous solutions of metal nitrates (10 mL/g support). The concentration of the metal-promoters oxides (15 wt% La_2O_3, 10 wt% CeO_2, and 15 wt% MgO, detailed in Table 1) supported over γ-Al_2O_3 was chosen to guarantee the maximum added amount of the promoter oxide maintaining a good dispersion, without the formation of large clusters of promoter oxides on the alumina surface. These amounts of La, Ce and Mg were previously optimized by studies carried out in our laboratories [20,21]. The impregnation was carried out during 1 h under stirring and water was removed under vacuum (150 mbar). The impregnated supports were dried under air at 100 °C for 12 h and subsequently calcined under air flow at 10 °C/min up to 800 (8 h), 650 (6 h) or 600 °C (6.5 h) for La-, Ce- and Mg-Al_2O_3 supports, respectively, following the previous studies [20,21].

Nickel was added over the X-modified alumina supports by wet impregnation method using a solution of $Ni(NO_3)_2{\cdot}6H_2O$ (*Aldrich*) with 10 mL distilled H_2O/g of support. The solvent was removed after 1 h under stirring by distillation under vacuum (150 mbar). The Ni/XA catalysts precursors were dried at 100 °C overnight and calcined under a flow of air from RT up to 500 °C for 5 h ($\Delta T/\Delta t$ = 10 °C/min). An additional catalyst (Ni/A), without metal oxide promoter, was prepared as reference material using the same method than that used for Ni/X-Al_2O_3 supports, in order to evaluate the effect of the addition of La-, Ce- and Mg-oxides to alumina support.

Bimetallic PtNi/XA catalysts were prepared by wet impregnation method using a solution of $Pt(NH_3)_4(NO_3)_2$ with 10 mL distilled H_2O/g of support (Ni/XA, for X = La, Ce or Mg). The PtNi/XA catalysts precursors were obtained after 1 h of impregnation under stirring, solvent removal by distillation under vacuum (150 mbar), drying at 110 °C overnight and vacuum (10–15 mbar) calcination at 300 °C for 3 h. Table 1 summarizes the nomenclature and chemical composition of the studied catalysts in this work.

2.2. Physicochemical characterization

2.2.1. Textural properties

Textural properties of X–Al (X = La, Ce, or Mg) supports and Ni- and PtNi-catalysts were obtained from the nitrogen adsorption isotherms. Nitrogen adsorption–desorption isotherms of the powdered samples were measured at −196 °C using a Micrometrics ASAP 2100 instrument. The specific surface area was calculated by the Brunauer–Emmett–Teller (BET) method. Prior to the measurements, the samples were outgassed under vacuum at 200 °C overnight.

2.2.2. X-ray diffraction (XRD)

XRD patterns of the powdered Ni- and Ni–Pt-precursors and fresh and used catalysts samples were recorded at room temperature on a Seifert XRD 3000P diffractometer using Cu Kα radiation (λ = 1.54056 Å). XRD patterns were collected in the range of 2θ from 5° to 95° (0.02°/step, integration time of 500 s/step). Identification of the phases was achieved by reference to the JCPDS diffraction data file. The reduced samples were prepared by reduction ex situ at 600 °C for 1 h with 10 vol% of H_2/Ar, subsequently, they were passivated with diluted oxygen doses, subsequently, extracted from reduction equipment and analyzed by XRD technique.

2.2.3. Temperature programmed reduction (TPR)

The samples (30 mg) for the TPR study were loaded in a U-shaped tubular quartz reactor which was heated by an electrical furnace on line with a Micromeritics TPD/TPR 2900 apparatus. The calcined precursors were reduced with 50 mL(STP)/min of a 10 vol% H_2/Ar reducing mixture. The temperature was progressively increased from room temperature (RT) up to 750 °C at a linearly programmed rate of 10 °C/min. A cold trap was placed at the outlet of the reactor to collect the water. The consumption of hydrogen was measured by comparison of the thermal conductivity difference between the reference and the product gas.

2.2.4. Temperature programmed ammonia desorption (TPD-NH_3)

The acidity of the Ni-catalysts were tested by chemisorbed ammonia desorption at temperature programmed using a Micromeritics Autochem II 2920 equipment with a TCD detector. Prior to ammonia chemisorption, the calcined materials were pretreated under He flow (50 mL(STP)/min) at 650 °C for 3 h (heating rate: 5 °C/min), in order to carry out the decomposition of surface carbonates which may have formed. The ammonia chemisorption was carried out at 90 °C for 1 h under a mixture of NH_3/He (50 mL(STP)/min of a 10 vol% NH_3/He mixture). The ammonia excess was eliminated at 110 °C with He (50 mL(STP)/min) flow for 1 h. Subsequently, the temperature was increased from 110 °C up to

Table 1
Nomenclature, chemical composition and textural characterization results of the fresh oxidized catalysts precursors.

Sample	Chemical composition						Textural result		
	Weight (%)			Atomic (%)			S_{BET} (m^2/g)	V_{pore} (cm^3/g)	D_{pore} (nm)
	Pt	NiO	XO	Pt	Ni	X			
γ-Al_2O_3	–	–	–	–	–	–	236	0.532	9
Ni/LaA	–	12	15 (La_2O_3)	–	9.5	5.5 (La)	113	0.524	18
Ni/CeA	–	12	10 (CeO_2)	–	9.3	3.4 (Ce)	177	0.650	14
Ni/MgA	–	12	15 (MgO)	–	8.3	19.1 (Mg)	110	0.412	15
PtNi/LaA	1	12	15 (La_2O_3)	0.3	9.5	5.5 (La)	119	0.348	11
PtNi/CeA	1	12	10 (CeO_2)	0.3	9.3	3.4 (Ce)	180	0.635	14
PtNi/MgA	1	12	15 (MgO)	0.3	8.3	19.1 (Mg)	119	0.399	12

750 °C ($\Delta T/\Delta t$ = 5 °C/min) with 50 mL(STP)/min of He flow to carry out the ammonia desorption.

2.2.5. X-ray photoelectron spectroscopy (XPS)

X-ray photoelectron spectra (XPS) of the fresh and used PtNi/X-A catalysts were acquired with a VG Escalab 200R spectrometer equipped with a hemispherical electron analyzer and an Mg Ka ($h\nu$ = 1253.6 eV) X-ray source. The peaks were fitted by a non-linear least square fitting program using a properly weighted sum of Lorentzian and Gaussian component curves after background subtraction according to Shirley and Sherwood. The constant charging of the samples was corrected by referencing all energies to the Al 2p peak at 74.5 eV.

2.2.6. Thermal gravimetric analysis (TGA)

The amount of carbon/coke produced during the acetone steam reforming was determined by thermogravimetric (TG) measurements obtained through the loss of weight during carbon combustion with a flow of air (100 mL(STP)/min) using a Mettler Toledo TGA/SDTA 851 thermalanalyser. The materials (10–15 mg) were heated from RT up to 750 °C at a linearly programmed rate of 10 °C/min.

2.2.7. Transmission electron microscopy (TEM)

Transmission electron microscopy (TEM) was used to study the used samples using a Philips Technai 20 microscope operating at 200 kV. The samples were ultrasonically dispersed in ethanol and transferred to carbon coated copper grids.

2.3. Acetone reforming testing

Steam reforming experiments were carried out in a continuous tubular fixed-bed quart reactor (I.D.: 7 mm) at atmospheric pressure using 0.500 mL (around 0.250 g) of each catalyst sieved to maintain a particle size between 425 and 600 μm. The samples were activated by reduction in situ at 600 °C (heating rate of 10 °C/min) for 1 h with 50 mL(STP)/min of a 10 vol% H_2/N_2 mixture. Subsequently, the reduced catalysts were tested in the acetone steam reforming reaction at atmospheric pressure with a mixing of H_2O/CH_3COCH_3 = 6.0 and N_2 = 41 vol%, GHSV = 10,180 h^{-1}. Activity tests were performed at 600 °C maintaining the reaction for 10 h. The reaction products were analyzed on-line by GC with TCD (Agilent) equipped with Porapack Q (CO_2, C_2H_6, C_2H_4, CH_2CO, water and acetone) and molecular sieve 5A (H_2, O_2, N_2, CO) packed columns connected in series, using He as carrier gas.

Activity data were reported as acetone conversion (XC_3H_6O), acetone gasification and selectivity to the different gasification products (Si), which are defined as follows:

$$XC_3H_6O\,(\%): [(\text{mole}\,C_3H_6O)_{in} - (\text{mole}\,C_3H_6O)_{out}]/(\text{mole}\,C_3H_6O)_{in} \times 100 \quad (2)$$

$$\text{gasification}\,(\%): \left(\sum \text{mol i}\right)_{out}/(3\,\text{mole}\,C_3H_6O)in \times 100, \quad i = CO,\ CO_2,\ CH_4 \quad (3)$$

$$Si\,(\%) = (\text{mole i})out/\left(\sum \text{mol i}\right)out \times 100, \quad i = H_2,\ CO,\ CO_2,\ CH_4,\ C_2H_4,\ C_2H_6,\ CH_2CO \quad (4)$$

3. Results

3.1. Characterization of precursors and catalysts

3.1.1. Textural properties

Table 1 summarizes the textural properties derived from N_2 adsorption–desorption isotherms of the calcined catalysts precursors. As observed in Table 1, the incorporation of a 15 wt% of lanthanum oxide in the Ni/LaA catalyst causes an important increase of the average pore size, while, as expected, a decrease of the surface occurs. The pore volume is almost constant, indicating that small pores have disappeared and have appeared larger size pores. Different is the case of Ni/CeA sample. This sample showed a lower decrease of the BET surface area and an increase of the pore volume that suggest the formation of intraparticle mesoporous volume, with higher porosity than in the case of the lanthanum counterpart. This fact agrees with the largest increase in average pore diameter obtained with the La-catalyst. In the case of the Ni/MgA catalyst the incorporation of Mg to Al_2O_3 implies a change in the textural properties of the alumina with a decrease in the pore volume together with an increase of the pore volume probably related with the formation of the Mg–Al phase (as detected by XRD analyses commented in the next section).

The incorporation of Pt to monometallic Ni/XA dos not causes modifications in the textural properties of Ce- and Mg-modified samples. However, the incorporation of Pt to Ni/LaA sample provokes a decrease in the average pore size and, consequently, in the pore volume, maintaining similar BET surface area than the corresponding monometallic Ni counterpart. This may be caused by the chemical treatment of the incorporation of Pt to the LaA sample, since during the Pt-impregnation stage the Pt precursor generates an acidic aqueous medium which modifies the LaA texture. The decrease in the average pore size, and pore volume, suggests that during this acid treatment, lanthanum could block the larger pores of the alumina support, thus reducing the pore volume.

3.1.2. X-ray diffraction (XRD)

Fig. 1 shows the XRD patterns of the Ni- and PtNi-oxidized catalyst precursors, together with the Ni/Al reference material. The characteristic peaks of poorly crystalline γ-Al_2O_3 (at 37.4°, 46.0° and 68.8° for JCPDS 4-875) were detected in the XRD pattern of the

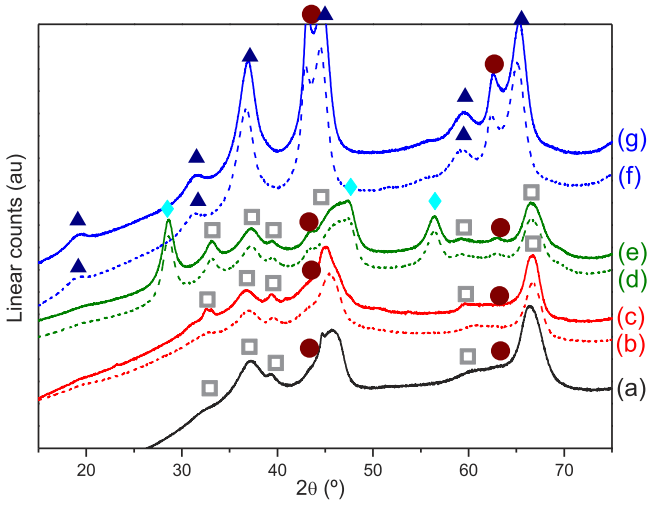

Fig. 1. XRD patterns of the oxidized catalysts precursors: (a), Ni/A, (b), PtNi/LaA, (c), Ni/LaA, (d), PtNi/CeA, (e), Ni/CeA, (f), PtNi/MgA, and (g), Ni/MgA. Detected phases: (□), γ-Al_2O_3 (JCPDS 4-875); (♦), CeO_2 (JCPDS 75-120); (▲), spinel (JCPDS 78-552); and (●), NiO and/or MgO (JCPDS 78-643 and 43-1022, respectively).

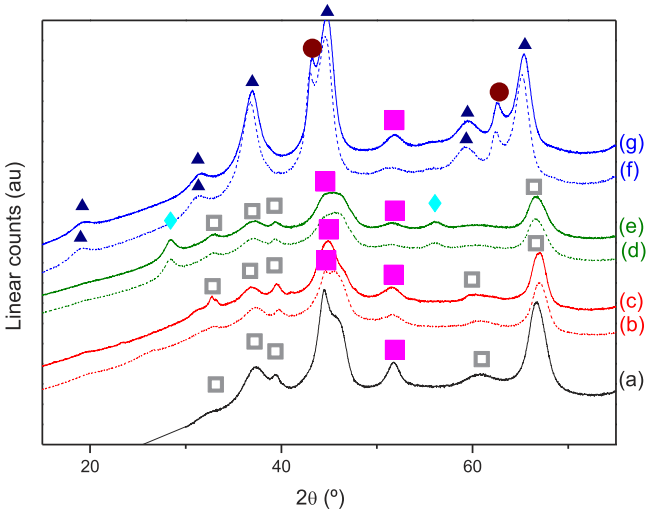

Fig. 2. XRD patterns of the reduced fresh catalysts: (a), Ni/A, (b), PtNi/LaA, (c), Ni/LaA, (d), PtNi/CeA, (e), Ni/CeA, (f), PtNi/MgA, and (g), Ni/MgA. Detected phases: (□), γ-Al_2O_3 (JCPDS 4-875); (♦), CeO_2 (JCPDS 75-120); (▲), spinel (JCPDS 78-552); (●), NiO and/or MgO (JCPDS 78-643 and 43-1022, respectively); and (■), Ni^0 metal (JCPDS 4-850).

Ni/Al reference. Likewise, the patterns of both Ce- and La-based catalysts show the γ-Al_2O_3 phase as main crystalline phase. No diffraction peaks corresponding to La-crystalline species of either La_2O_3 (JCPDS 83-1355) or $LaAlO_3$ (JCPDS 85-1071) were observed on La-based catalyst. This is not surprising because lanthanum exists in the form of a two-dimensional overlayer on alumina, which cannot be detected by XRD for lanthanum loadings up to 8.5 μmol La/m^2 [23], for LaA material 0.96 μmol La/m^2. XRD patterns of the Ce-based samples show reflections corresponding to CeO_2 crystalline phase, which suggests the segregation of the Ce-phase over the Al_2O_3 surface.

Regarding the Ni-phases, the reference Ni/Al sample and both Ce- and La-supported precursors show poor defined Ni peaks corresponding to the NiO phase (JCPDS 78-643), which is the only Ni-phase detected. The presence of $NiAl_2O_4$ would be difficult to determine by this technique, since the diffraction lines of this spinel phase are coincident with those of the γ-Al_2O_3 (with pseudospinel structure). Ni- and PtNi-supported on CeA present poor defined peaks at 43.5° and 63° corresponding to NiO-crystalline phase. However, the Ni/A reference material and the monometallic and bimetallic precursors supported on LaA, only show one shoulder around 43.5° (corresponding to the most intense (2 0 0) lattice plane of NiO-phase). The crystallite size of NiO was estimated by application of Scherrer equation (Table 2) to the diffraction peak of NiO at 63° because is the diffraction line with less overlapping with the intense peaks corresponding to alumina phase. However, the overlap of the (2 2 0) lattice plane at 63° peak of NiO-phase with the corresponding to the alumina (5 1 1) and (4 4 0) at 61° and 67° peaks, respectively, complicates to estimate the NiO particle size for Ni/A and Ni/LaA samples. The quantitative estimation of crystallite sizes of NiO phase for the Ni/CeA sample seems to show larger crystal size than that suggested by the Ni/LaA pattern. For bimetallic PtNi samples, it is observed that the Pt addition lightly decreases the NiO particle size for both Ce- and La-based materials. The systematic decrease of the NiO crystallite size after the Pt-addition could be caused by a re-dispersion of NiO particles during the Pt-impregnation process. In all bimetallic PtNi samples no diffraction peaks corresponding to Pt-phases were detected, which indicates the small Pt-particle size, which was expected given the low Pt loading added to these materials (Table 1). Therefore, it could also be a sign of the high dispersion of Pt species, since no periodic structures higher than 3 nm are detected by XRD.

Ni/and PtNi/MgA samples show different XRD patterns than those described for La- and CeA supported counterparts. The main phase observed on Ni/MgA sample is the spinel of Ni–Al or Ni,Mg–Al. The small size of Mg^{2+} and Ni^{2+} cations favors their incorporation into the Al^{3+} structure forming the (Ni)Mg–Al spinel. Together with the spinel phase, the corresponding peaks of the NiO (JCPDS 78-643) and/or MgO (JCPDS 43-1022) phases can be detected. The complete coincidence of the diffraction lines of the MgO and NiO phases makes the discrimination among both phases not possible. Bimetallic PtNi/MgA sample shows the same XRD profile than that observed on monometallic Ni counterpart, indicating that the Pt-addition does not modify the crystalline structure of monometallic Ni/MgA samples. No diffraction peaks related to Pt phases were detected in bimetallic PtNi calcined catalyst.

Fig. 2 shows the XRD patterns of the Ni- and PtNi-reduced fresh catalysts at 600 °C for 1 h with 10 vol% of H_2/Ar, together with the Ni/Al reference material reduced in the same conditions. After reduction, all catalysts show the reflections corresponding to reduced Ni metallic phase. The XRD pattern of the Ni/Al reference shows only two crystalline phases: the Ni metallic one and the most intense phase corresponding to the alumina support. For the La- and Ce-modified catalysts, the diffraction peaks corresponding to NiO disappeared after reduction which suggests the complete reduction of the NiO phase detected on the calcined catalyst precursors. In the case of MgA supported catalysts is most difficult to analyze the evolution of NiO phase after reduction because the complete coincidence of the diffraction lines of the MgO and NiO phases. In the reduced MgA supported catalysts, the metallic Ni^0 phase appears after the reduction observing a decrease in the linear counts corresponding to the NiO + MgO peak at 63° relative to the linear counts of the peak of the spinel phase at 65°. This relative decrease of the linear counts of the NiO + MgO peak suggests the reduction of the supported NiO phase. Apparently, none support was modified during the reduction process.

The crystallite size of the Ni^0 phase has been calculated by application of Scherrer equation to the diffraction peak at 53.8° (Table 2), to avoid overlap with other peaks alumina. The low XRD reflections corresponding to metallic Ni phases may lead to some inaccuracies in the determination of absolute crystalline sizes. Nevertheless, quantitative estimation of crystallite sizes by applying the Scherrer equation after a careful mathematical treatment of diffraction

Table 2
Main phases and average particle size of crystalline Ni phases detected on the fresh oxidized catalysts precursor, the reduced catalysts and the used catalyst from XRD.

Sample	XRD of the samples[a]						
	Precursor oxidized			Reduced catalysts		Used catalysts	
	Main	Others	t_{NiO} (nm)	Ni-phase	t_{Ni} (nm)	t_{Ni} (nm)	Graph. linear counts[b] (au)
Ni/A	Al_2O_3	NiO(traces)	–	Ni^0	30	45	11,957
Ni/LaA	Al_2O_3	NiO(traces)	–	Ni^0	15	20	5370
Ni/CeA	CeO_2/Al_2O_3	NiO	10	Ni^0	12	30	1980
Ni/MgA	Spinel	NiO + MgO	7	Ni^0/spinel/NiO + MgO	15	ND	ND
PtNi/LaA	Al_2O_3	ND	–	Ni^0	10	15	ND
PtNi/CeA	CeO_2/Al_2O_3	NiO	8	Ni^0	6	25	1265
PtNi/MgA	Spinel	NiO + MgO	6	Ni^0/spinel/NiO + MgO	7	20	510

ND: not detected.
[a] XRD phases detected: γ-Al_2O_3 (JCPDS 4-875), CeO_2 (JCPDS 75-120), NiO (JCPDS 78-643), MgO (JCPDS 43-1022), spinel (JCPDS 78-552), Ni^0 (JCPDS 04-850) and C (JCPDS 41-1487).
[b] Linear counts of the characteristic graphite peak at 26°.

patterns allows achieving the accuracy degree necessary for comparative purposes. Quantitative estimation of crystallite sizes of Ni^0 phase (Table 2) indicates the similar crystallite size of Ni^0 entities for monometallic samples irrespective of the composition of the support, except for the reference Ni/A material which shows a high metallic Ni particle size (Table 2), regarding to the poorly defined NiO peaks (Fig. 1). This result proves the importance of the promoter oxides presence which increases the metallic Ni dispersion avoiding the sinterization during the reduction treatment. Crystalline sizes for Ni^0 particles in reduced samples were higher than NiO crystalline size on calcined catalysts indicating some nickel sintering phenomena during the reduction process. Bimetallic reduced catalysts showed metallic Ni particles smaller than the monometallic counterparts. Thus, it seems that the presence of Pt on catalysts prevents sintering of Ni particles during the activation treatment. Crystalline size for Ni^0 particles in reduced bimetallic catalysts varies with the support and decreasing according the order: Ni/LaA > Ni/MgA > Ni/CeA.

3.1.3. Temperature programmed reduction (TPR)

The H_2 consumption profiles corresponding to the TPR experiments performed on the calcined precursors are shown in Fig. 3. TPR data showed differences in reduction temperatures of the Ni in each samples together with differences in the amount of hydrogen consumed (Table 3), which are linked to the relative proportion of nickel species reduced for each material depending on the support used to disperse the nickel entities.

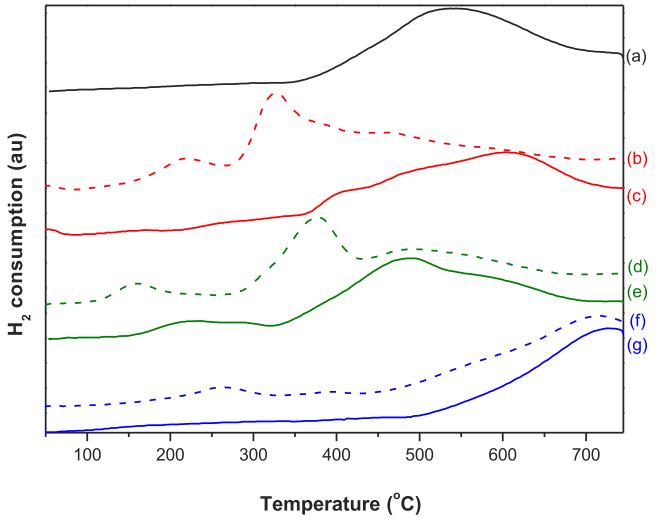

Fig. 3. TPR profiles of the supported oxidized mono- and bimetallic catalysts precursors: (a), PtNi/LaA, (b), Ni/LaA, (c), PtNi/CeA, (d), Ni/CeA, (e), PtNi/MgA, (f), Ni/MgA, and (g) Ni/A.

The TPR profile of the Ni/Al reference material shows an only broad peak at 536 °C (Table 3). The high reduction temperature, at temperature close to 500 is related to the reduction of amorphous mixed oxides or highly dispersed non-stoichiometric amorphous nickel aluminate spinels [24,25]. This high reduction temperature indicates the strong interaction of Ni with the alumina support, beyond only be deposited on the support surface. Therefore, this high temperature required for Ni reduction indicates the partial incorporation of Ni in the alumina structure.

The monometallic Ni catalysts supported on modified-alumina show different performance as a function of the oxide present in the support. The incorporation of La to Al_2O_3 support increases the reduction intensity of NiO species with a weak interaction with the support from 400 °C, which is the temperature assigned to the typical reduction of Ni^{2+} in NiO species with weak interaction with alumina [26–28]. The reduction peak at higher temperatures, 500 °C and 600 °C, are related to the reduction of highly dispersed non-stoichiometric amorphous nickel aluminate spinels [24,25] and to a diluted $NiAl_2O_4$-like phase respectively [29–31]. Bulk spinel typically reduces at higher temperature [32], whereby the absence of peaks up to 700 °C indicates the non-formation of bulk spinel phases. For this sample it is also observed an increase in the proportion of diluted $NiAl_2O_4$ (peak up to 600 °C), which is the main reduction component for this sample (Table 3), at the expense of the highly dispersed non stoichiometric amorphous nickel aluminate phase (peak at 480 °C, Table 3, Fig. 3), as can be seen by comparing the reduction profile of Ni/LaA sample with the reduction profile of Ni/A sample (Fig. 3). In the catalyst supported on CeA, the highly dispersed non stoichiometric amorphous nickel aluminate or NiO species with a strong interaction with the support (at 487 °C in Table 3) seem to be the most abundant phases. In this sample it is also observed small reduction components at 220 °C and 290 °C, which could be ascribed to the reduction of isolate ceria species (not detected by XRD) while the bulk CeO_2 species (detected by XRD) are maintained after the reduction process at 750 °C, as it is

Table 3
TPR characterization results of the catalysts precursors.

Catalysts	T_{max} (°C)	$T_{components}$ (°C)	H_2 consumption (μmol/g_{cat})
Ni/Al	540	–	4.68
Ni/LaA	670	400/480	4.69
Ni/CeA	487	220/290/590	4.60
Ni/MgA	732	–	5.91
PtNi/LaA	325	215/470	5.20
PtNi/CeA	375	160/490	4.97
PtNi/MgA	730	265	5.26

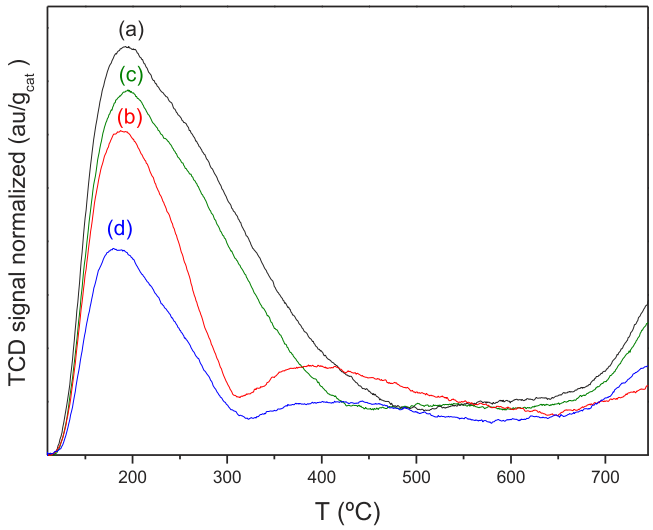

Fig. 4. TPD-NH_3 profiles of the supported oxidized mono-metallic catalysts precursors: (a), Ni/A, (b), Ni/LaA, (c), Ni/CeA, and (d), Ni/MgA.

possible to detect in oxidized samples (by XRD in Fig. 1) and in reduced samples (Fig. 2). In the case of the monometallic Ni sample supported on Mg-modified Al_2O_3 support, the reduction temperature of Ni species shift up to 700 °C as consequence of the incorporation of Ni ions into the Mg–Al spinel matrix that is difficult to reduce.

The reduction profiles of bimetallic PtNi catalysts show changes respect to the monometallic counterparts. For the PtNi/LaA and PtNi/CeA catalysts, the most intense H_2 consumption peak is centered at 325 °C and 375 °C respectively (Table 3). An additional peak at 215 °C (for La-bimetallic catalyst) and 160 °C for Ce-ones (Table 3) is detected for both samples. Additionally, a broad peak at 470 and 490 °C is observed for PtNi/LaA and PtNi/CeA catalysts, respectively. The peaks at low temperature comprise the reduction of PtO_x species while the consumption peaks observed in the region of 300–700 °C include the reduction of Ni species with different degrees of interaction with the support, as well as surface $NiAl_xO_y$. It is remarkable that the reduction of this type of Ni^{2+} species was recorded at temperatures ca. 120 °C lower than in the monometallic Ni counterparts. This phenomenon is attributed to a promoting effect of Pt on the reducibility of Ni species, in good agreement with the literature [33], which seems to indicate a high degree of contact between Ni (which is reduced) and Pt on the surface LaA and CeA materials. Finally, the reduction profile of the bimetallic PtNi/MgA appeared unchanged respect to the reduction behavior observed in the monometallic Ni/MgAl catalyst, indicating that the presence of Pt on the surface cannot affect the reducibility of Ni species into the Mg–Al spinel matrix. In this case, the possible contact between Ni and Pt is lower due to Ni is included into the Mg–Al matrix.

3.1.4. *Temperature programmed ammonia desorption (TPD-NH_3)*

Fig. 4 shows the ammonia TPD profiles of the oxidized monometallic catalysts precursors. The amount of ammonia desorbed during the temperature programmed desorption is linked to the acidity of each material. As expected, the addition of promoter oxides on the surface of alumina in all cases decreases the acidity of the original support (γ-Al_2O_3). Thus, the increasing order of acidity of the precursors follows the trend: Ni/MgA (2.87 cm^3 of NH_3/g of catalyst) < Ni/LaA (3.72 cm^3 of NH_3/g of catalyst) < Ni/CeA (6.83 cm^3 of NH_3/g of catalyst) < Ni/A (8.28 cm^3 of NH_3/g of catalyst), as shown in Fig. 4. Ni/MgA precursor shows the lowest acidity, retaining only 35% of the original acidity. The formation of the basic (Ni,Mg)–Al-spinels decreases the acidity of the original alumina support. Different is the case of the Ni/LaA material. The La-based precursor shows 45% of the original acidity. This low acidity could be due to the high dispersion of the promoter oxide on the alumina surface, which is suggested by the absence of the La-oxides characteristic XRD peaks (Fig. 1). The large size of the La_2O_3 molecules together with the good dispersion of the oxide on the surface of the support, guarantee the decrease in acidity of the material with respect to the starting alumina. This results support this assumption. Finally, the Ni/CeA sample exhibits the highest acidity of the modified materials Ni/XA, maintaining 85% of the acidity of the original alumina. The low acidity loss detected for this precursor can be due to poor dispersion of CeO_2 on the alumina surface, which is suggested by the results of XRD (Fig. 1, Table 2). These results hint at the agglomeration of Ce (to make visible its crystal by XRD) reduces the loss of acidity regarding the alumina one.

The additional broad band at higher temperature in the TPD profiles appear for Ni/MgA and Ni/LaA materials could be caused by isolated clusters of alumina, which increase its acidity by the isolation.

3.1.5. *X-ray photoelectron spectroscopy (XPS)*

The binding energies of Al 2p, (La 3d, Ce 3d or Mg 2p), Ni 2p, Pt 4d, and C 1s core-levels have been recorded for the oxidized bimetallic catalysts precursors and the results are listed in Table 4.

Ni 2p binding energy of all fresh oxidized samples is located at higher values (around 256 eV) than the corresponding to NiO phase at 854.0 eV [17]. That means that Ni^{2+} presents strong interactions with the support surface, including the inclusion of Ni cation into Al-matrix. XRD results proved the presence of like-spinel structure, which binding energy is reported near to 856.9 eV [17], which is a value much closer to our experimental results. Therefore, the main contribution for the Ni 2p surface signal is due to this like-spinel type species. These results are in agreement with that observed by TPR. The reduction temperatures are for phase with Ni incorporated to Al-matrix, for all catalysts. The Pt 4d peak displays a component at 315–316 eV associated to a metal phase (Pt^0), and another one located at 318 eV originated from oxidic platinum species, likely PtO_2 [17]. The La 3d peak envelopes were centered at 835.6 eV, which is close to the values reported for well-dispersed La-species on alumina, which agrees with the XRD and TPD-NH_3 results. The C 1s peak of the fresh PtNi/MgA sample displays components at 277.1 and 278.8 eV arise from highly structured carbon, while peaks at 280.8 and 282.7 eV originate from amorphous carbon, which can be assigned to Mg-carbonate.

The surface atomic ratios of the calcined samples, calculated from the intensities of the XPS peaks are also summarized in Table 4. The high dispersion of lanthanum on the alumina surface or high coating of alumina by lanthanum (two facts related to each other) observed for the LaA material is corroborated by the high atomic ratio regarding the theoretical value (X/Al in Table 4). By contrast, the catalyst with Ce shows atomic ratios below its theoretical value, which implies a low dispersion of this oxide on alumina surface. The analysis of the Mg-sample is difficult, because the formation of spinel makes not possible to speak of “dispersion or coating”, as both Mg and Ni seem to be incorporated into the structure of the surface spinel (detected by XRD and XPS).

3.2. *Acetone steam reforming tests*

To evaluate the contribution of the thermal decomposition of acetone, the homogeneous (non-catalytic) steam reforming of acetone at 600 °C was firstly investigated. Under the steam reforming conditions, acetone was converted in small extent (3.3%). The main products observed from the thermal conversion of acetone were methane and ketene (results not shown here). Small amount of coke (<0.05%) was observed demonstrating that acetone was thermally

Table 4
Binding energies (eV) of core electrons and surface atomic ratios of fresh and used bimetallic PtNi/X–Al (X = La, Ce and Mg) catalysts.

Catalyst	Binding energies (eV)						Surface atomic ratios				C (%)
	Al2p[a]	O1s	Ce3d La3d Mg2p	Ni2p	C1s	Pt4d	X/Al	Ni/(X + Al)	Pt/(X + Al)	Pt/(Ni + X + Al)	
Theoretical							0.065	0.105	0.0033	0.0030	–
PtNi/LaA	74.5	531.5	835.6	856.1	–	315.4 (38) 318.0 (62)	0.097	0.244	0.0042	0.0042	–
PtNi/LaA-used	74.5	531.5	835.4	852.3 (24) 856.0 (76)	~278[b]	N.D.	0.136	0.177	N.D.	N.D.	13.4
Theoretical							0.044	0.115	0.0037	0.0033	–
PtNi/CeA	74.5	531.5	882.5	856.5	–	316.0 (51) 318.1 (49)	0.022	0.110	0.0018	0.0016	–
PtNi/CeA-used	74.5	531.5	882.3	856.0	279.9	N.D.	0.043	0.037	N.D.	N.D.	14.6
Theoretical							0.690	0.177	0.0064	0.0054	–
PtNi/MgA	74.5	531.5	50.2	856.3	284.8 (62) 289.7 (38)	314.9 (37) 316.6 (32) 318.4 (31)	0.543	0.128	0.0029	0.0026	2.1[c]
PtNi/MgA-used	74.6	531.7	50.2	854.4 (18)* 856.2 (82)	277.1 (44) 278.8 (19) 280.8 (17) 282.7 (13) 284.8 (7)	N.D.	0.664	0.113	N.D.	N.D.	40.3

N.D. = not detected.
[a] The samples with La and Mg exhibited charging effects, binding energies were calibrated taking Al2p peak at 74.5 eV.
[b] Carbon deposits on the catalyst surface showed a much larger charging effect than that of catalyst elements.
[c] Mg carbonate.

decomposed to coke to a limited extent under steam reforming conditions used in this study.

The conversion of acetone and the distribution of products for the steam reforming of acetone over monometallic Ni/XA and bimetallic PtNi/XA catalysts are plotted in Figs. 5 and 6, respectively. The selectivity to products achieved at steady state (10 h on stream) is displayed in Table 5.

All catalysts showed complete conversion of acetone being H_2, CO, CO_2 and CH_4 the only gas products detected (Table 5). As it is observed in Figs. 5 and 6, all catalysts showed a stable distribution

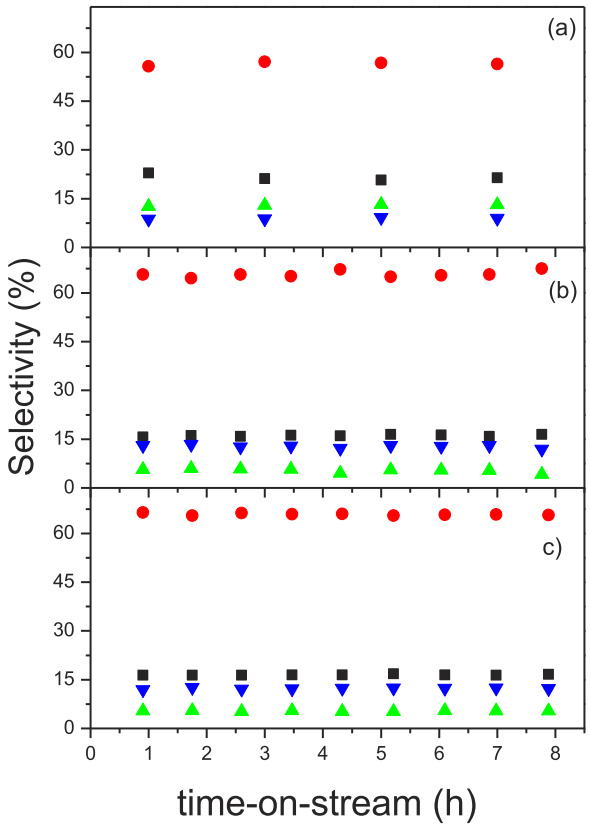

Fig. 5. Selectivity to gas products during acetone steam reforming over monometallic Ni/XA catalysts (873 K, H_2O/CH_3COCH_3 = 6.0, GHSV = 10,180 h^{-1}): (a), Ni/LaA, (b), Ni/CeA and (c), Ni/MgA (● H_2, ■ CO_2, ▲ CH_4, ▼ CO).

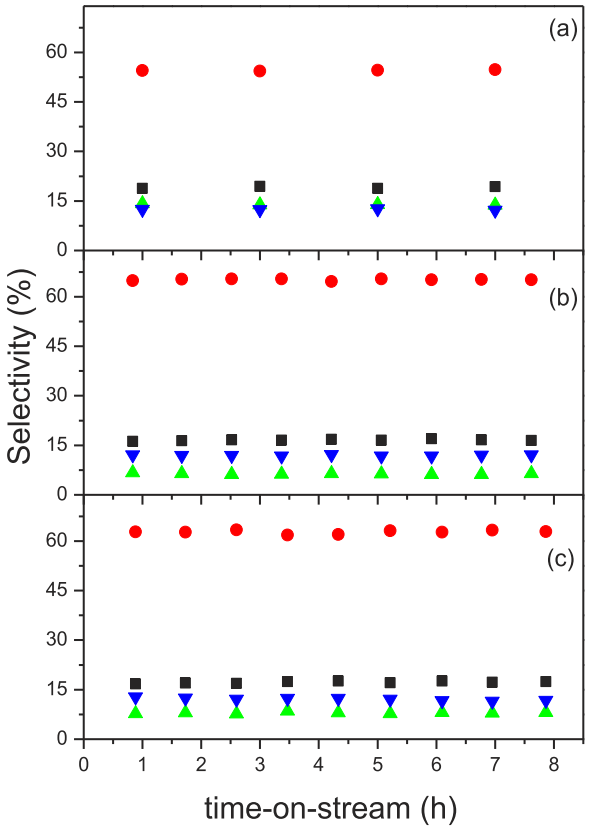

Fig. 6. Selectivity to gas products during acetone steam reforming over bimetallic PtNi/XA catalysts (873 K, H_2O/CH_3COCH_3 = 6.0, GHSV = 10,180 h^{-1}): (a), PtNi/LaA, (b), PtNi/CeA and (c), PtNi/MgA (● H_2, ■ CO_2, ▲ CH_4, ▼ CO).

Table 5
Selectivity toward products in acetone steam reforming after 10 hours on stream over samples corresponding to fourth catalysts series (873 K, H_2O/CH_3COCH_3 = 6.0, GHSV = 10,180 h^{-1}).

Catalysts	Acetone conversion (%)	Gasification (%)	Gasification products selectivity (%)				Thermogravimetry	
			H_2	CO_2	CO	CH_4	Coke ($mg_C/g_{cat}/h$)	T (°C)
Ni/A	100	77.3	67	16	5	12	27.53	590
Ni/LaA	100	94.1	57	20	9	14	20.25	590
Ni/CeA	100	81.4	66	16	5	13	24.14	590
Ni/MgA	100	85.9	66	17	5	12	14.86	575
PtNi/LaA	100	99.8	53	20	12	15	0.05	–
PtNi/CeA	100	84.9	65	17	6	12	23.53	590
PtNi/MgA	100	87.3	63	17	8	12	13.71	580

of reaction products with reaction time. However, the gasification capacity and selectivity to products obtained over the different catalysts depend on the composition of support and also on the presence of Pt in the catalyst composition. Gasification capacity of catalysts increases when Pt is present and it also increases with the support used according to the following sequence: CeA < MgA < LaA. The observed changes in the gasification capacity of catalysts are related with changes in the reaction routes that lead to coke/oligomer products. Acetone can undergo aldol condensation and oligomerization reactions on catalysts with acid and/or basic sites as well as hydrogenation on metallic sites. Aldol condensation of acetone to diacetone alcohol (DAA) is catalyzed by either basic or acid sites, while the dehydration of diacetone alcohol (DAA) to mesityl oxide (MO) is acid-catalyzed and the selective hydrogenation of mesityl oxide (MO) requires metal sites. At high temperatures, these products can suffer secondary oligomerization reactions leading to numerous higher condensation products which form deposits on catalysts surfaces. Therefore the differences in gasification observed in the tested catalysts imply that catalysts formulation modifies in different way the routes of formation of coke/oligomers products. Taking into the account the importance of the distribution of coke/oligomers products, these non-gasification products have been estimated and plotted together with the selectivity to all products (H_2, CO_2, CH_4, CO and oligomers/coke) achieved at steady state in Fig. 7. Together with the selectivity to oligomers + coke, the amount of coke determined by TG is also plotted in Fig. 7 directly as wt% (right y). From this figure it is observed that amount of coke + oligomers produced varies with type of support decreasing in the order of A > CeA > MgA > LaA. This sequence is similar to that obtained for the acidity of the materials determined by TPD-NH_3, suggesting that the formation of these oligomers is favored by the acidity of the material. The presence of Pt in the catalyst formulation also decreases the production of coke + oligomers on catalysts, showing the sample PtNi/LaA the lower formation of these products among the tested catalysts.

Evolution of the selectivity to gas products also depends on the composition of support and also on the presence of Pt in the catalyst formulation (Fig. 7). Monometallic Ni catalysts supported on CeA and MgA showed higher hydrogen selectivity with lower selectivity to CO and CH_4 than that observed for Ni/LaA catalyst (Table 5). This product distribution was indicative of an enhancement in the C—H bond breaking and water gas shift capacity the higher water gas shift capacity with the presence of Mg and Ce in the support formulation. On the other hand, the bimetallic PtNi catalysts showed similar product selectivity than that observed on monometallic Ni counterparts, except for slight differences in the selectivity to CO.

3.3. Characterization of used catalysts

3.3.1. X-ray diffraction (XRD)

The X-ray diffraction profiles of catalysts used in the steam reforming of acetone reaction are displayed in Fig. 8. The XRD profiles of used catalysts are similar than those of the reduced catalysts (Fig. 2) showing the characteristic diffraction peaks associated to the supports (mainly alumina), which suggests that not structural modifications of the supports are produced under reforming conditions. Regarding to evolution of Ni^0 species after reaction, crystallite sizes of metallic nickel in the used catalysts obtained by applying the Scherrer equation were calculated (Table 2). The size of metallic Ni crystallites observed for monometallic Ni- and bimetallic

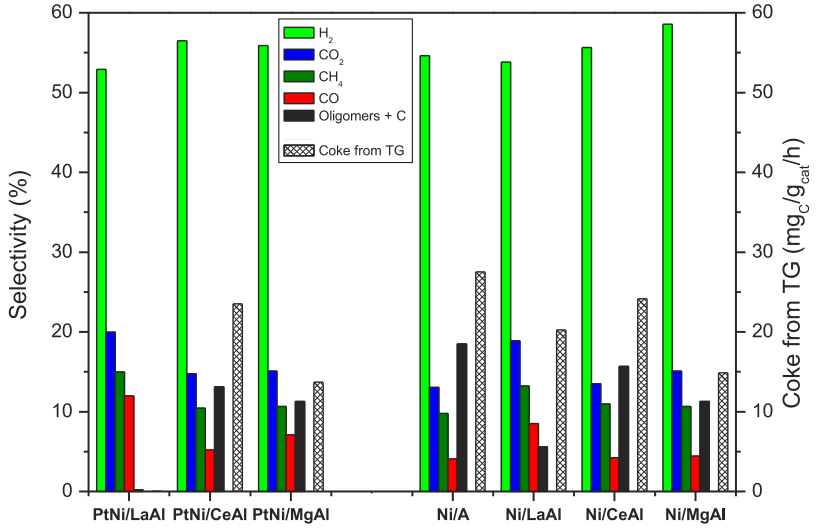

Fig. 7. Catalytic results of Ni/XAl, PtNi/XAl and Ni/A reference after 10 h on the acetone steam reforming at 873 K, H_2O/CH_3COCH_3 = 6.0, GHSV = 10,180 h^{-1}.

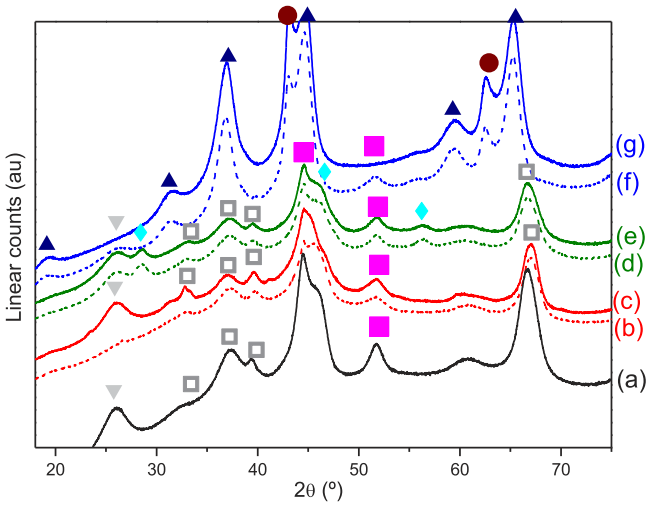

Fig. 8. XRD patterns of the used catalysts in the acetone steam reforming reaction: (a), Ni/A, (b), PtNi/LaA, (c), Ni/LaA, (d), PtNi/CeA, (e), Ni/CeA, (f), PtNi/MgA, and (g), Ni/MgA. Detected phases: ( ), γ-Al_2O_3 (JCPDS 4-875); ( ), CeO_2 (JCPDS 75-120); ( ), spinel (JCPDS 78-552); ( ), NiO and/or MgO (JCPDS 78-643 and 43-1022, respectively); ( ), Ni^0 metal (JCPDS 4-850); and ( ), carbon-graphite (JCPDS 41-1487).

PtNi-catalysts was larger than that calculated on reduced fresh samples, pointing that sintering of metallic Ni crystallites has occurred under reforming conditions on these catalysts. The sintering effect is different depending on the composition of support and presence of Pt in the formulation. The Ni/A reference catalyst sinterizes regarding the reduced fresh ones, although the higher agglomeration is produced during the reduction process. The increase of crystal size is lower during the catalytic process. Catalysts supported on CeA show the highest growth of particle size, suggesting a poor stabilization of Ni metal on this support, which can be caused by the poor dispersion of the Ce-particles (XRD and XPS results) that they cannot avoid the Ni-sintering. On the contrary, the LaA support showed a low degree of sintering with respect to the reduced fresh catalysts, indicating the better stabilization of Ni^0 particles on this support during the reforming process. This better stabilization seems to be linked to the higher La-dispersion over alumina.

In addition to these phases, the diffraction patterns of the used Ni/A, Ni/LaA, Ni/CeA, PtNi/CeA and PtNi/MgA catalysts showed lines at 2θ angle of 26° characteristic of graphitic carbon (JCPDS 75-1621). This fact indicates that coke deposition took place during the acetone steam reforming over these catalysts. The intensity of the signal at 26° characteristic of graphitic carbon deposit depends on the chemical formulation of the catalyst used (Table 2), increasing in the order: Ni/MgA = PtNi/LaA < PtNi/MgA ≪ PtNiCeA < NiCeA < Ni/LaA < Ni/A. This order is related to the crystallinity of the produced coke. The presence of graphitic coke is particularly important in the cases of the Ce-based catalysts and monometallic Ni/LaA sample. On the contrary, the bimetallic PtNi/LaA and the monometallic Ni/MgA catalysts did not show diffraction peaks related to graphitic carbon indicating the limited amount of carbon formed on this sample.

3.3.2. Thermogravimetric analysis (TGA)

Thermogravimetric analyses of the used samples were carried out to quantify the carbonaceous residues formed by measuring the weight loss during their temperature programmed oxidation. Coke combustion begins for all catalysts at 350 °C and reaches its maximum at temperatures between 575 and 590 °C depending on the catalysts composition. The combustion terminates in all cases at 650 °C. The high combustion temperatures indicated the high graphitic degree of the coke deposited on catalyst surfaces. In particular, the Ni/A, Ni/LaA, Ni/CeA and PtNi/CeA used catalysts exhibit the highest combustion temperature at 590 °C (Table 5). These results are in agreement with those observed by XRD on used samples (Table 2 and Fig. 8). On the contrary, the lowest combustion temperature was obtained for the Ni/MgA used sample (575 °C), in which the XRD characteristic graphitic peak at 26° was not detected. Therefore, it seems that there is a relationship between the XRD peak intensity of graphite at 26° and the combustion temperature determined by TGA. Comparing the amount of coke formed on used catalysts, it can be inferred that Pt plays an important role in diminishing carbon production under reaction only in the case of the PtNi/LaA sample.

3.3.3. Transmission electron microscopy (TEM)

Fig. 9 shows the TEM micrographs of three representative samples of the used catalysts. Micrographs of used catalysts showed similar morphologies in all cases. The used catalysts presented Ni particles with some carbon agglomerations on surface. The presence of carbon agglomerates is particularly important in the case of the used Ni/CeA and PtNi/CeA used samples, while in the case of used PtNi/LaA counterpart the formation of agglomerates of carbon seems to have place in much lesser extension. In all used samples the formation of carbon nanostructures during the acetone steam reforming was not observed.

On the other hand, differences in the Ni^0 particles size could be observed in used samples. Ni metal particles with sizes between 6 and 25 nm can be observed in the used catalysts, being the La-catalyst the sample that shows particles of smaller size and the CeA supported catalysts the sample with larger particles.

3.3.4. X-ray photoelectron spectroscopy (XPS)

The results of the XPS analysis of the bimetallic used catalysts are listed in Table 4. The Ni 2p peak binding energy of all used samples is located at 856 eV, which is assigned to the spinel or like-spinel structures. The only two exceptions were: PtNi/MgA, which shows an additional component at 856 eV (assigned to NiO, probably produced by the passivation of metal Ni); and PtNi/LaA which shows a component at 852 eV, assigned to Ni^0.

Regarding the surface chemical composition, there is a systematic decrease in the Al surface exposed regarding the promoter oxide (X/Al in Table 4) for all binary catalysts. Likewise, a loss of Ni on the surface is observed. This Ni-loss is probably due to encapsulation of Ni particles by produced coke. The Pt 4f peak is not detected. The loss of Pt in the used samples probably indicates that Pt has been covered by deposits of coke.

4. Discussion

Reforming activity results obtained on Ni and Pt–Ni catalysts supported on modified Al_2O_3 showed that both metal and support, play an essential role in their catalytic behavior on the steam reforming of acetone reaction. The acidic sites of the X-modified-Al_2O_3 supports could react with acetone adsorbed on these sites by means of condensation/oligomerization reactions whereas both nickel and platinum activate the organic fragments by means of O—H, C—C and C—H bond breaking and promoting their reaction with the OH groups from the water. Thus, the higher acidity of the A and CeA materials seems to be linked to the higher yield to the condensation/oligomerization products, together with the higher amount of coke deposited.

The sequence of gasification capacity over monometallic samples (Ni/LaA > Ni/MgA > Ni/CeA > Ni/A) points out that acidity of supports participates in the acetone reforming mechanism over these catalysts. Ce-containing support showed a relatively low gasification capacity (81.4%) which indicates the high extension of the

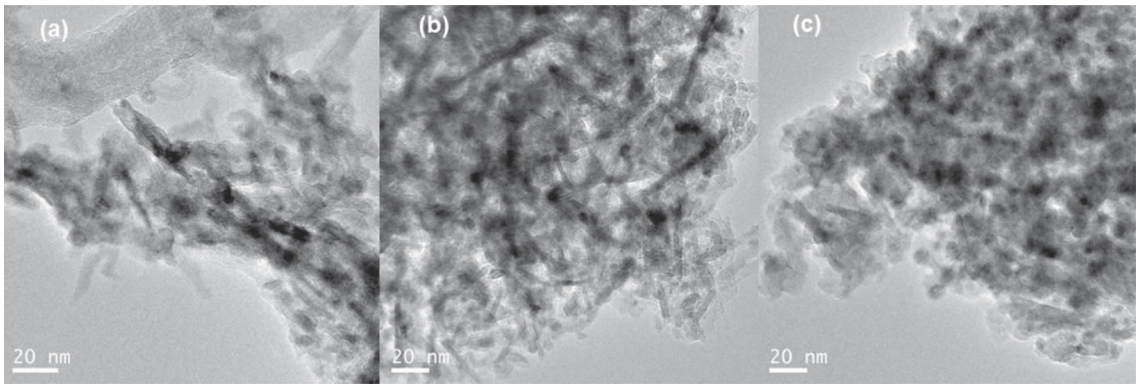

Fig. 9. TEM micrographs of the (a), Ni/CeA, (b), PtNi/CeA, and (c), PtNi/LaA used catalysts.

condensation/oligmerization reactions on the support, in which its high acidity plays an important role. Moreover, characterization of Ni/CeA catalyst showed a low dispersion of the Ce entities on the catalyst surface with segregation of CeO_2 particles which may be the cause of the low gasification activity of this catalyst as consequence of the low blockage of the acid sites of alumina by Ce entities. On the contrary, the monometallic Ni/LaA catalyst showed high gasification capacity as it gasifies 94% of the acetone feed (Table 4). Characterization results by XRD on Ni/LaA catalyst showed homogeneous dispersion of La on the Al_2O_3 support that probably have partially blocked in higher extension the surface acid sites of alumina responsible of the oligomerization/condensation reactions. In the case of the Ni/Mg–A catalyst, this sample shows a low gasification capacity in spite of the high dispersion of Mg species achieved over the Al_2O_3 support of this sample. The low gasification capacity of the Ni/MgA could be related with the lower capacity of the Mg ions to block the surface acid sites of alumina in comparison with La or Ce as it was showed in our previous work [20] or to the high reactivity of the Mg–Al spinel formed for the acetone condensation/oligomerization reactions due to its high basicity [34].

Analysis of product distribution observed in the reforming of acetone on monometallic Ni/XA samples indicates differences in the reforming capacity of the samples. Samples Ni/MgA and Ni/CeA showed similar reforming capacity being they higher than that presented by Ni/LaA counterpart. Taking into account that all catalysts showed similar Ni particles size on the fresh reduced samples (Fig. 2, Table 2), the observed differences in reforming capacity may arise from the different capacity of the support to participate in the reforming reaction. It is know that enhanced adsorption of water by ceria and magnesium may increase the available surface OH groups to promote the reforming reactions [21,35]. Therefore the better reforming capacity observed on Ni/MgA and Ni/CeA can be attributed to this fact.

Significant amounts of coke were observed on Ni/CeA and Ni/LaA catalysts while in the monometallic sample supported on Al_2O_3 modified with Mg the formation of carbon was lower (Table 5). On Ni–Mg catalysts applied to hydrocarbon reforming, the interaction between nickel and magnesium species is suggested to prevent coke deposition by enhanced adsorption of water by magnesium species may increase the available surface oxygen to promote the surface oxidation reactions of carbon precursors on metal particles, thereby inhibiting carbon growth on the catalyst surface. Close Ni–Mg interaction was observed in Ni/MgA sample as XRD and TPR demonstrated showing the inclusion of Ni into the Mg spinel matrix. It is also know that on Ni–La and Ni–Ce catalysts, the interaction between nickel and lanthanum or cerium species prevent the coke deposition, however, it is not the case in our samples. The high extension of coke formation on Ni/LaA and Ni/CeA could be ascribed to the low interaction of Ni with La and Ce species developed on these samples as TPR and XRD results indicated (Figs. 2 and 3).

Addition of Pt to monometallic Ni catalysts only has a beneficial effect in the reforming capacity of the Ni/LaA sample. TPR profiles in Fig. 3 showed that on bimetallic catalysts Pt strongly enhanced the reducibility of Ni species on Ce- and La-modified supports. According to XRD results, bimetallic reduced catalysts showed metallic Ni particles smaller than the monometallic counterparts. Crystalline size for Ni^0 particles in reduced bimetallic catalysts varies with the support and decreasing according the order: Ni/LaA > Ni/MgA > Ni/CeA. In spite of this fact, it is observed that Pt has only beneficial effect in the activity and stability of the Ni active phase when is supported on La-modified Al_2O_3. XRD analyses on used NiPt bimetallic samples pointed to the existence of strong sintering of Ni crystallites during the steam reforming reaction on PtNi/CeA and PtNi/MgA catalysts. On the contrary, the bimetallic PtNi catalyst supported on LaA showed a low degree of sintering with respect to the reduced fresh catalysts, indicating the better stabilization of Ni^0 particles on this support during the reforming process. The higher stability of Ni particles at the surface of PtNi catalyst modified with lanthanum might explain its good gasification capacity in the acetone steam reforming. The improvement in reforming activity can be also originated by the differences in coke formation when Pt is present in the catalyst formulation. Comparing the amount of coke formed over PtNi catalysts (Table 5), it is clear that Pt only plays an important role in diminishing carbon production under reaction on the PtNi/LaA catalyst. Significant amounts of coke were observed on PtNi/CeA and PtNi/MgA catalysts while in sample supported on Al_2O_3 modified with La the formation of carbon was markedly suppressed. It is know that both the metallic Ni particle size and the Pt play a major role in assisting coke removal. In this sense, Ni particles of smaller size detected on LaA support favor low carbon deposition while platinum assists in coke removal enhancing the mobility of the H-atoms formed in the reaction for the gasification of coke intermediates formed during the acetone reforming [22].

5. Conclusions

Steam reforming of acetone (as representative molecule of bio-oil) to produce H_2 was investigated over bimetallic Pt–Ni catalysts supported on alumina modified with Ce, La and Mg oxides. Physicochemical characterization showed that metal-support interactions and the size of metallic Ni at surface differ depending on the oxide added to the alumina support. Comparison between Pt–Ni catalysts and monometallic Ni counterpart points out that Pt only enhances the Ni reducibility on supports modified with Ce and La. The presence of Pt only stabilizes the Ni^0 particles on the support modified with La during the reforming process. Reforming

activity results obtained on Ni and Pt–Ni supported on alumina modified with Ce, La and Mg oxides to be compared with Ni/A ones, showed that both metal and support, play an essential role in their catalytic behavior on the steam reforming of acetone reaction. The sequence of gasification capacity over monometallic samples (Ni/LaA > Ni/MgA > Ni/CeA) points out that acidity of supports participates in the acetone reforming mechanism over these catalysts. Analysis of product distribution observed in the reforming of acetone on monometallic Ni samples indicates differences in the reforming capacity of the samples. Samples Ni/MgA and Ni/CeA showed similar reforming capacity being they higher than that presented by Ni/LaA counterpart. Addition of Pt to monometallic Ni catalysts only has a beneficial effect in the reforming capacity of the Ni/LaA sample, due to the promoting effect of Pt that leads to an increase in the stability of metallic Ni particles on catalyst surface.

Acknowledgements

This research was supported by the Ministry of Science and Innovation (Spain) and the Autonomous Government of Madrid, Madrid (Spain) under grants ENE2010-21198-C04-01 and S2009ENE-1743, respectively. Partial support to this work came from Najran University, The Kingdom of Saudi Arabia.

References

[1] S. Wang, F. Zhang, Q. Cai, X. Li, L. Zhu, Q. Wang, Z. Luo, Int. J. Hydrogen Energy 39 (2014) 2018–2025.
[2] T. Chen, C. Wu, R. Liu, Bioresour. Technol. 102 (2011) 9236–9240.
[3] S. Sarkar, A. Kumar, Bioresour. Technol. 101 (2010) 7350–7361.
[4] S. Czernik, R. French, C. Feik, E. Chornet, Ind. Eng. Chem. Res. 41 (2002) 4209–4215.
[5] S. Czernik, R. Evans, R. French, Catal. Today 129 (2007) 265–268.
[6] M. Marquevich, S. Czernik, E. Chornet, D. Montané, Energy Fuels 13 (1999) 1160–1166.
[7] A.C. Basagiannis, X.E. Verykios, Appl. Catal. A 308 (2006) 182–193.
[8] F. Cheng, V. Dupont, Int. J. Hydrogen Energy 38 (2013) 15160–15172.
[9] X. Hu, G.X. Lu, Appl. Catal. B: Environ. 88 (2009) 376–385.
[10] M.C. Ramos, A.I. Navascues, L. Garcia, R. Bilbao, Ind. Eng. Chem. Res. 46 (2007) 2399–2406.
[11] D. Wang, D. Montane, E. Chornet, Appl. Catal. A: Gen. 143 (1996) 245–270.
[12] E.Ch. Vagia, A.A. Lemonidou, Appl. Catal. A: Gen. 351 (2008) 111–121.
[13] P.N. Kechagiopoulos, S.S. Voutetakis, A.A. Lemonidou, I.A. Vasalos, Energy Fuels 20 (2006) 2155–2163.
[14] Z. Li, X. Hu, L. Zhang, S. Liu, G. Lu, Appl. Catal. A: Gen. 417–418 (2012) 281–289.
[15] B. Matas Güell, I. Babich, K.P. Nichols, J.G.E. Gardeniers, L. Lefferts, K. Seshan, Appl. Catal. B: Environ. 90 (2009) 38–44.
[16] K. Takanabe, K. Aika, K. Seshan, L. Lefferts, Top. Catal. 49 (2008) 68–72.
[17] R.M. Navarro, R. Guil-Lopez, J.M. Gonzalez-Carballo, A. Cubero, A.A. Ismail, S.A. Al-Sayari, J.L.G. Fierro, Appl. Catal. A: Gen. 474 (2014) 168–177.
[18] K. Takanabe, K. Aika, K. Seshan, L. Lefferts, J. Catal. 227 (2004) 101–108.
[19] W.T. Reichle, J. Catal. 63 (1980) 295–306.
[20] M.C. Sanchez-Sanchez, R.M. Navarro, J.L.G. Fierro, Int. J. Hydrogen Energy 32 (2007) 1462–1471.
[21] R.M. Navarro, M.C. Alvarez-Galvan, M.C. Sanchez-Sanchez, F. Rosa, J.L.G. Fierro, Appl. Catal. B: Environ. 55 (2005) 229–241.
[22] M.C. Sanchez-Sanchez, R.M. Navarro, D.I. Kondarides, X.E. Verykios, J.L.G. Fierro, J. Phys. Chem. A 113 (2010) 3873–3879.
[23] M. Bettman, R.E. Chase, K. Otto, W.H. Weber, J. Catal. 117 (1989) 447–454.
[24] K.Y. Koo, H. Roh, Y.T. Seo, D.J. Seo, W.L. Yoon, S.B. Park, Appl. Catal. A 340 (2008) 183–190.
[25] J. Juan-Juan, M.C. Román Martínez, M.J. Illán-Gómez, Appl. Catal. A 355 (2009) 27–32.
[26] J.M. Rynkowski, T. Paryjczak, M. Lenik, Appl. Catal. A: Gen. 106 (1993) 73–80.
[27] N. Ichikuni, D. Murata, S. Shimazu, T. Uematsu, Catal. Lett. 69 (2000) 33–37.
[28] J.T. Richardson, M.W. Twigg, Appl. Catal. A: Gen. 167 (1998) 57–69.
[29] M.L. Dieuzeide, V. Iannibelli, M. Jobbagy, N. Amadeo, Int. J. Hydrogen Energy 37 (2012) 14926–14930.
[30] A. Parmaliana, F. Arenas, F. Frusteri, N. Giordano, J. Chem, Soc Faraday Trans 86 (1990) 2663.
[31] S.L. Gonzalez-Cortes, I. Aray, M.A. Rodulfo-Baechler, C.A. Lugo, H.L. Del Castillo, A. Loaiza-Gil, F.E. Imbert, H. Figueroa, W. Pernıa, A. Rodrıguez, O. Delgado, R. Casanova, J. Mendialdua, F. Rueda, J. Mater. Sci. 42 (2007) 6532–6540.
[32] H. Özdemir, M.A. Faruk Öksüzömer, M. Ali Gürkaynak, Int. J. Hydrogen Energy 35 (2010) 12147–12160.
[33] M. El Doukkali, A. Iriondo, P.L. Arias, J. Requies, I. Gandarias, L. Jalowiecki-Duhamel, F. Dumeignil, Appl. Catal. B: Environ. 125 (2012) 516–529.
[34] K. Pupovac, R. Palkovits, Chem. Sus. Chem. 6 (2013) 2103–2110.
[35] S. Natesakhawat, R.B. Watson, X.Q. Wang, U.S. Ozkan, J. Catal. 234 (2005) 496–508.